Rational Design of MnO/Carbon Nanopeapods with Internal Void Space for High-Rate and Long-Life Li-Ion Batteries

Hao Jiang,[†] Yanjie Hu,[†] Shaojun Guo,[‡,*] Chaoyi Yan,[§] Pooi See Lee,[§] and Chunzhong Li[†,*]

[†]Key Laboratory for Ultrafine Materials of Ministry of Education, School of Materials Science and Engineering, East China University of Science and Technology, 130 Meilong Road, Shanghai 200237, China, [‡]Physical Chemistry and Applied Spectroscopy, Los Alamos National Laboratory, Los Alamos, New Mexico 87545, United States, and [§]School of Materials Science and Engineering, Nanyang Technological University, Singapore 639798, Singapore

ABSTRACT Searching the long-life MnO-based materials for lithium ion batteries (LIBs) is still a great challenge because of the issue related to the volumetric expansion of MnO nanoparticles (NPs) or nanowires (NWs) during lithiation. Herein, we demonstrate an unexpected result that a peapod-like MnO/C heterostructure with internal void space can be facilely prepared by annealing the MnO precursor (MnO-P) NW/polydopamine core/shell nanostructure in an inert gas, which is very different from the preparation of typical MnO/C core/shell NWs through annealing MnO NW/C precursor nanostructure. Such peapod-like MnO/C heterostructure with internal void space is highly particular for high-performance LIBs, which can address all the issues related to MnO dissolution, conversion, aggregation and volumetric expansion during the Li^+ insertion/extraction. They are highly stable anode material for LIBs with a very high reversible capacity (as high as 1119 mAh g^{-1} at even 500 mA g^{-1}) and fast charge and discharge capability (463 mAh g^{-1} at 5000 mA g^{-1}), which is much better than MnO NWs (38 mAh g^{-1} at 5000 mA g^{-1}) and MnO/C core/shell NWs (289 mAh g^{-1} at 5000 mA g^{-1}). Such nanopeapods also show excellent rate capability (charged to 91.6% in 10.6 min using the constant current mode). Most importantly, we found that MnO/C nanopeapods show no capacity fading even *after 1000 cycles* at a high current density of 2000 mA g^{-1}, and no morphology change. The present MnO/C nanopeapods are the most efficient MnO-based anode materials ever reported for LIBs.

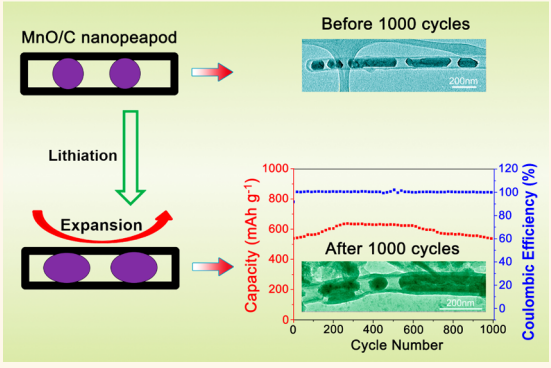

KEYWORDS: MnO nanowire · nanopeapod · lithium ion battery · heterostructure · anode material

The development of high power-density and long cycle-life rechargeable lithium ion batteries (LIBs) is a key for the future electric vehicles.[1−9] To meet the ever-increasing performance demands, the search for high-performance anode materials (*i.e.*, high capacity and desired stability) is urgent in building the next-generation LIBs.[1−5] Among different anode materials, MnO has attracted much attention recently because of its low conversion potential, low voltage hysteresis (<0.8 V), high theoretical capacity (756 mAh g^{-1}), natural abundance, environmentally benign and low electrochemical motivation force (emf) (1.032 V *vs* Li/Li^+).[10−12] However, like other transition metal oxides, the intrinsically low conductivity of MnO makes it suffer from poor rate capability. Specifically, the biggest issue of MnO materials for LIBs is that they can react with lithium to form metal Mn (dispersed in the Li_2O matrix), resulting in drastic volumetric change and severe capacity fading after only a few discharge/charge cycles.[10,13,14] Coating or hybridizing MnO materials with advanced carbon nanomaterials provides an advanced avenue for enhancing the power and energy densities and initially improving the stability. This is because carbon nanomaterials can greatly enhance the conductivity of MnO, and besides, the elastic feature of carbon materials can effectively relieve the strain caused by the volumetric change during lithiation/delithiation process, partly improving their cycling stability. These hybrid

* Address correspondence to czli@ecust.edu.cn, shaojun.guo.nano@gmail.com.

Received for review March 6, 2014 and accepted May 14, 2014.

Published online May 14, 2014
10.1021/nn501310n

strategies have been demonstrated on the synthesis of MnO/C core/shell nanorods,[12,15] MnO NPs attached on graphene[16,17] and hollow porous MnO/C microspheres, *etc.*[10,18] Despite their great potentials, the integrity maintenance of these materials during continuous charge/discharge cycles is still unsatisfactory due to very limited elasticity of carbon on intact MnO/C core/shell nanostructure or graphene supported MnO NPs. This brings a critical problem because crack and fracture of the carbon coating layer could emerge as a result of the volumetric expansion of MnO core, rendering the conventional core/shell morphology ineffective in keeping MnO integrity for long-life LIBs, and resulting in its limited cycle life of less than 100 cycles and low Coulombic efficiency. Therefore, the discovery of new materials with extremely high stability and high power and energy densities for LIBs is much needed for satisfying their practical applications.

Herein, we demonstrated a new process for the facile synthesis of novel heterostructured MnO/C nanopeapods with internal void space by virtue of the difference on crystallization degree of poor-crystalline MnO-P NWs and well-crystalline MnO NWs. The poor crystallization of MnO-P NW in MnO-P/polydopamine (PDA) core/shell nanostructure made it more easily broken into NPs during the carbonation process at high temperature, while under the same condition, the morphology of well-crystalline MnO NWs in MnO/C core/shell NWs could be well kept. In our unexpected nanopeapods, MnO NPs (less than 100 nm in diameter) were confined in carbon nanotubes (CNTs) with wall thickness of ~15 nm. The nanopeapods have a large void volume ratio of about 20.6% between the adjacent MnO NPs within the CNTs. We found that such particular nanostructure based on nanopeapods can address several important challenging issues related to LIBs: (a) improving the electronic conductivity of MnO through the use of conducting carbon as a shell, (b) reducing the dissolution and aggregation of MnO NPs during electrochemical process (Figure 1a,b) and (c) providing large enough room for the expansion upon lithiation (Figure 1c). As a consequence, this type of MnO-based hybrids exhibit a maximum specific capacity of 1119 mAh g^{-1} at high rate of 500 mA g^{-1} with outstanding charge/discharge rate capability (463 mAh g^{-1} at 5000 mA g^{-1}) and long cycle life (>1000 cycles without any decrease), demonstrating a great potential as anode materials for LIB applications. The present heterostructured MnO/C nanopeapods are the most efficient MnO-based materials ever reported for LIBs to date.

RESULTS AND DISSUSION

Material Design and Structure Characterization. Figure 2a shows the typical preparation process for the synthesis of the MnO/C nanopeapods and MnO/C core/shell NWs. First, MnO-P NWs and single-crystalline MnO NWs were synthesized through polyvinylpyrrolidone

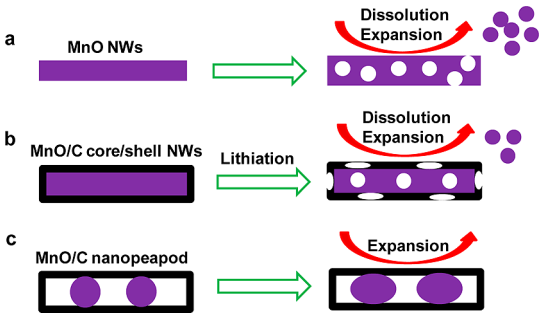

Figure 1. (a) Pure MnO NWs suffer from great volume expansion and dissolution during lithiation, leading to fast capacity fading. (b) Volumetric expansion of MnO NW in MnO/C core/shell NWs during lithiation causes the fracture of carbon shell, resulting in MnO dissolution as well. (c) The MnO/C nanopeapods provide enough internal void space for accommodating the volume expansion of MnO during Li^+ insertion, ensuring the structural integrity.

(PVP)-assisted hydrothermal treatment of $KMnO_4$ and the thermal decomposition of $MnCO_3$ NWs in argon,[19] respectively. The original MnO-P NWs have the black color (Figure S1a, Supporting Information) and show the weak XRD peaks (Figure S2, Supporting Information, not clear for the actual crystalline structure of MnO precursor). These MnO-P NWs were not stable under high temperature and could be transformed into different products depending on the use of temperature. For instance, annealing MnO-P NWs at 500 °C for 3 h made them have brown color, different from the original black color of MnO-P NWs (Figure S1b, Supporting Information). While single-crystalline MnO NWs have the stable green color (Figure S1c, Supporting Information), even at high temperature (data not shown), and show the strong (111), (200), (220), (311) and (222) diffraction peaks of MnO (JPCD card: 78−0424) (Figure S2, Supporting Information). These well-crystalline MnO NWs with the diameter of ~80 nm (Figure S3, Supporting Information) are highly stable in the inert gas. Then, these MnO-P and MnO NWs were used as templates to self-polymerize dopamine on their surface to get MnO-P NW/PDA and MnO NW/PDA core/shell nanostructures. Finally, the as-prepared MnO-P (or MnO) NW/PDA core/shell nanostructure was carbonized at high temperature in an inert gas to prepare MnO/C nanostructure.

We are amazing to find that during the carbonization process, the MnO-P NWs were broken into MnO NPs (Figure 2b,c and Figure S4, Supporting Information), and MnO/C nanopeapods with large internal void space were formed. Figure S5 (Supporting Information) shows the typical XRD patterns of the as-prepared MnO/C nanopeapods (blue) and MnO/C core/shell NWs (red). All the three samples have the same diffraction peaks located at 34.9°, 40.7°, 58.9°, 70.3° and 73.9°, which can be assigned to the face-centered cubic (*fcc*) MnO (JCPDS, file no. 78−0424). No other characteristic peaks from impurities are observed, indicating the effective

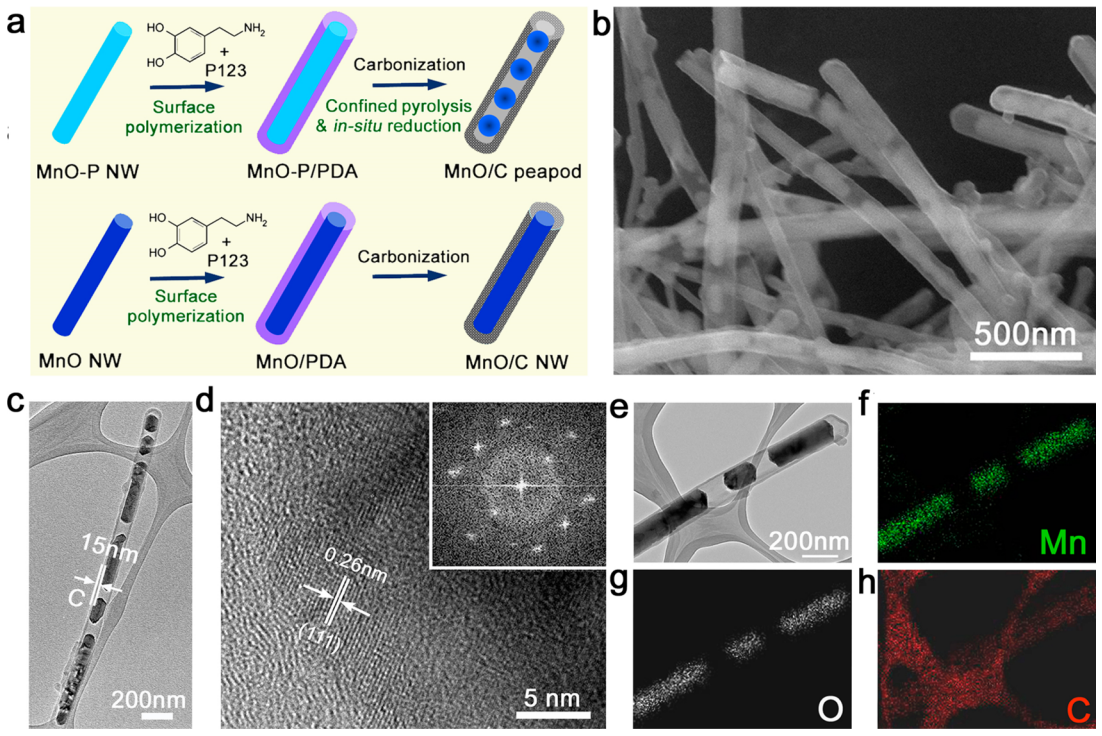

Figure 2. (a) Schematic illustration on the preparation of the heterostructured MnO/C nanopeapods and MnO/C core−shell NWs. (b) SEM image, (c) TEM image, (d) HRTEM image (the inset showing the corresponding FFT image), and (e−h) TEM-EDS mapping of the heterostructured MnO/C nanopeapods.

formation of MnO-based materials. The scanning electron microscopy (SEM, Figure 2b) and transmission electron microscopy (TEM) images (Figure S4, Supporting Information) of the MnO/C nanopeapods indicate that MnO NPs are well-confined in CNTs, forming a peapod-like morphology. Such a structure can provide a large void space of about 20.6% between the two adjacent NPs. A representative heterostructured MnO/C nanopeapod is shown in Figure 2c. The thickness of the carbon layer is determined to be ~15 nm. From the well-resolved lattice fringes of the high-resolution TEM (HRTEM) image (Figure 2d) taken from the edge of one nanopeapod, an interplanar spacing of 0.26 nm is obtained, being consistent with the distance of the (111) plane of the cubic MnO.[20] The corresponding fast Fourier transformation (FFT) pattern (inset of Figure 2d) can also be assigned to the cubic structure. These results suggest that single MnO NP confined in CNTs is single-crystalline nature. Elemental distribution of a representative MnO/C nanopeapod is investigated by TEM-energy dispersed spectroscopy (EDS) mapping, as seen in Figure 2e−h. Along the nanopeapod, Mn and O distribute intermittently across the whole peapod, clearly displaying the gaps between two MnO NPs, whereas C uniformly distributes on the whole peapod. This further indicates the formation of MnO/C nanopeapods.

It is noteworthy that the formation of our MnO/C nanopeapod is very different from that obtained from annealing MnO NW/PDA core/shell nanostructure, in which the morphology of MnO NWs in core/shell nanostructure can be well maintained after high-temperature annealing treatment (Figure S6, Supporting Information). We found that the MnO-P NWs show the weaker XRD diffraction peak than the MnO NWs, proved by XRD results (Figure S2, Supporting Information). Such relatively poor crystallinity of MnO-P NWs probably make them not stable at high temperature (*e.g.*, color change), thus enabling them much more easily broken into NPs during the reduction and transformation of the unstable MnO_x precursor into MnO by the shell under high-temperature carbonization. Such nanopeapods are highly particular for possibly enhancing the performance of LIBs due to the additional introduction of internal void space for volumetric expansion during lithiation.

The carbon content of the as-prepared MnO/C nanopeapods is evaluated by inductively coupled plasma (ICP) elemental analyses, EDS and thermogravimetric analysis. ICP result shows that the carbon content in nanopeapods is determined to be about 16.1%, which is in accordance with those of the EDX (15.0%) and TGA results (15.6%) (Figure S7, Supporting Information, for the detailed analysis). Raman spectroscopy was further used to evaluate the graphitic quality of the MnO/C nanopeapds, as shown in Figure 3a. Two obvious peaks around 1363 and 1595 cm^{-1} are observed, corresponding to the disordered carbon (D-bond) and the ordered graphitic carbon (G-bond), respectively.[21] The I_D/I_G intensity ratio is calculated to be 0.89, smaller than that of reduced graphene,[22]

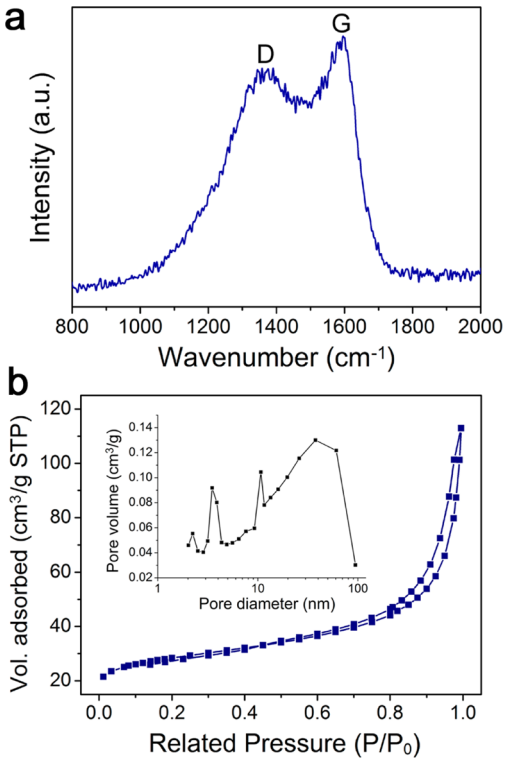

Figure 3. (a) Raman spectrum and (b) N_2 adsorption–desorption isotherms of the heterostructured MnO/C nanopeapods. The inset of (b) shows the corresponding pore-size distribution curve.

indicating a high degree of graphitization of the carbon shell in the nanopeapods. This is favorable to improve the electrical conductivity. N_2 adsorption/desorption isotherm and the pore size distribution are shown in Figure 3b. The Brunauer–Emmett–Teller (BET) surface area of MnO/C nanopeapods is measured to be about 103 $m^2\ g^{-1}$, higher than those of previously reported MnO-based materials (Table S1, Supporting Information). Such a large specific surface area is important for enhancing the power/energy density of LIBs. The nanopeapods have a multimodal mesopore size distribution (inset of Figure 3b) of big cavity (>10 nm) from the void space between adjacent MnO NPs and small pore (<4 nm) from the carbon shell. Such a multimodal pore structure will be helpful to accommodate the volumetric change during the lithiation/delithiation process, giving rise to a relatively high capacity and excellent cycling stability.

Electrochemical Performance. The electrochemical performance of the MnO/C nanopeapods, MnO/C core/shell NWs and pure MnO NWs was evaluated by assembling these materials into coin-type 2016 cells, respectively. The working electrode was prepared by mixing individual sample with conductive carbon black and poly(vinyldifluoride) (PVDF) binder in *N*-methyl-2-pyrrolidinone (NMP) to form a slurry, followed by casting it onto copper foil and drying overnight in a vacuum. Lithium foil was used as counter electrode. The cyclic voltammograms (CVs) of the MnO/C nanopeapods within the potential range of 0.02–3 V at a scan rate of 0.1 mV s^{-1} are shown in Figure 4a. In the cathodic scan, two peaks at 0.22 and 0.70 V are observed in the first cathodic scan, corresponding to the initial reduction of MnO to metallic Mn ($MnO + 2Li^+ + 2e^- \rightarrow Mn + Li_2O$) and the formation of a solid electrolyte interface (SEI), respectively. During the anodic scan, only one peak around 1.28 V is observed due to the MnO formation ($Mn + Li_2O \rightarrow MnO + 2Li^+ + 2e^-$) and Li_2O decomposition.[12,23] The corresponding peaks centered at 0.22 and 1.28 V then shifted to 0.47 and 1.31 V for the subsequent cathode/anode scans, respectively, probably owing to the enhanced kinetics and active materials utilization of the hybrid electrode arising from the microstructure change after the first lithiation.[24–26] The cyclic voltammograms (CVs) of MnO/C nanopeapods are basically overlapped in the second and third cycles, indicating good reversibility during the electrochemical process. The first five charge and discharge curves of MnO/C nanopeapods have been provided in Figure S8 (Supporting Information), showing a high Coulomb efficiency of ~88% at the first cycle.

The rate capability of MnO/C nanopeapods was also explored, as shown in Figure 4b. The assembled cell using nanopeapods as active materials is first tested at the same charge and discharge current densities of 100 mA g^{-1}, and then at increased current densities from 200 to 5000 mA g^{-1}. The nanopeapods deliver a high average capacity of 845 mA h g^{-1} at 100 mA g^{-1}. Even when measured at a very high current density of 5000 mA g^{-1}, a high capacity of 463 mAh g^{-1} can still be obtained (~55% retention). After the deep charge/discharge for 5 cycles at 5000 mA g^{-1}, an average capacity of 940 mA h g^{-1} is recovered when scanned again at 100 mA g^{-1}. As comparisons, the pure MnO and MnO/C core/shell NWs exhibit lower capacities of 322 and 687 mAh g^{-1}, respectively at 100 mA g^{-1}, with poor rate capability (the capacities of only 38 and 289 mAh g^{-1} for MnO and MnO/C core/shell NWs at 5000 mA g^{-1}, respectively). And most importantly, the LIB performance of MnO/C nanopeapods is greatly enhanced compared to those of the previously reported MnO/C coaxial nanocables,[15,27] hollow porous MnO/C microspheres[10,13] and even many graphene-based MnO hybrid materials.[20,23,25] Besides, the capacity of MnO/C nanopeapods (1119 mAh g^{-1} at 500 mA g^{-1}) is higher than the theoretical capacity of both MnO (756 mAh g^{-1}) and graphite (372 mAh g^{-1}). This can be ascribed to the strong synergistic effect between MnO core and carbon shell.[4] Another reason may be related to the generation of Mn^{4+} during charge/discharge process because the fact that the Mn^{2+} in the MnO/C nanopeapods could be partly reoxidized to a higher oxidation state (Mn^{4+}),[28,29] which was proved by the X-ray photoelectron spectroscopy (XPS) (Figure S9a,b, Supporting Information) and CV results (Figure S9c,

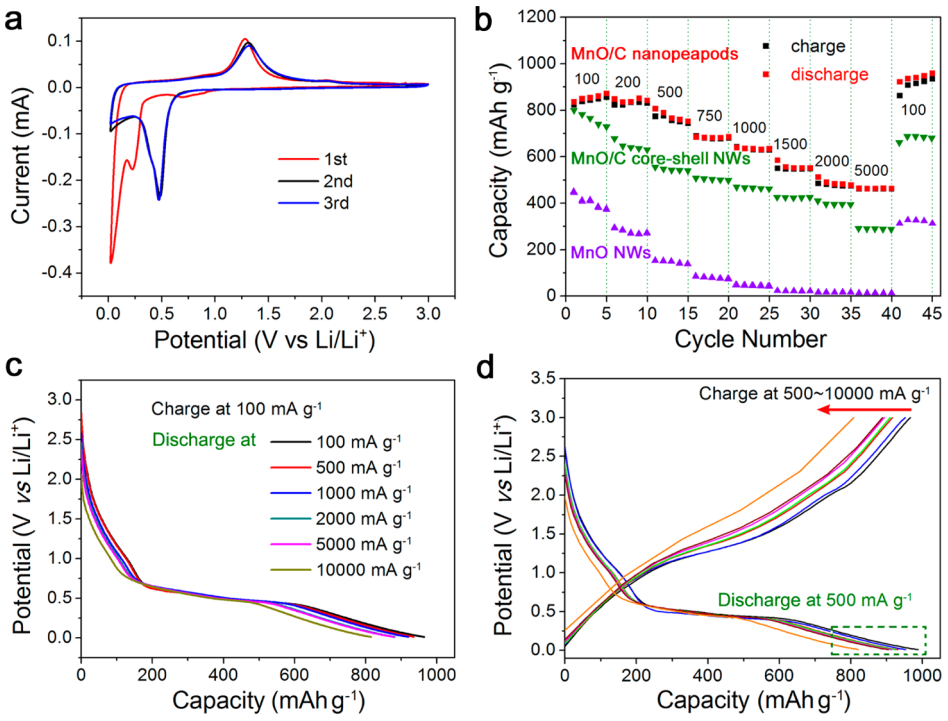

Figure 4. (a) CVs of the MnO/C nanopeapods for the first three cycles at a scan rate of 0.1 mV s^{-1}, (b) the capacity retention of the MnO/C nanopeapods, MnO/C core/shell NWs and pure MnO NWs at various current densities, (c) the discharge curves of the MnO/C nanopeapods from 100 to 10 000 mA g^{-1} under the constant charge current density of 100 mA g^{-1}, and (d) the discharge curves of MnO/C nanopeapods at 500 mA g^{-1} under high charge current densities from 500 to 10 000 mA g^{-1}.

Supporting Information) of the MnO/C nanopeapods after over 1000 cycles (detailed analysis shown in the Supporting Information).

To evaluate the discharge rate performance, the cells are charged at a constant current density of 100 mA g^{-1} and then discharged at various current densities ranging from 100 mA g^{-1} to 10 000 mA g^{-1} (Figure 4c). The MnO/C nanopeapods retain 95.4, 91.1 and 84.5% of the initial capacity at the discharge current densities of 1000, 5000 and 10 000 mA g^{-1}, respectively. They exhibit an excellent discharge rate capability even at super high discharge current density of 10 000 mA g^{-1}, which is the best retention so far for MnO-based anode materials. The charge rate performance is also investigated by setting the discharge rate constant to 500 mA g^{-1} and then increasing the charge rates from 500 to 10 000 mA g^{-1} (Figure 4d). They exhibit a discharge capacity of 988 mAh g^{-1} after 500 mA g^{-1} charging. The capacity can maintain 905 and 821 mAh g^{-1} at 5000 and 10 000 mA g^{-1} charging, respectively. These results imply that the MnO/C nanopeapods can be rapidly charged to 91.6% in 10.6 min and 83.1% in 4.9 min using the constant current mode of 500 mA g^{-1}. Such excellent rate capabilities may potentially bring significant impact on the development of electric vehicles and smart grids.

Figure 5 shows the Ragone plots of MnO/C nanopeapods, calculated from Figure 4b,c. Under the same charge/discharge rates, the energy density is estimated to be 434 Wh kg^{-1} when the power density is

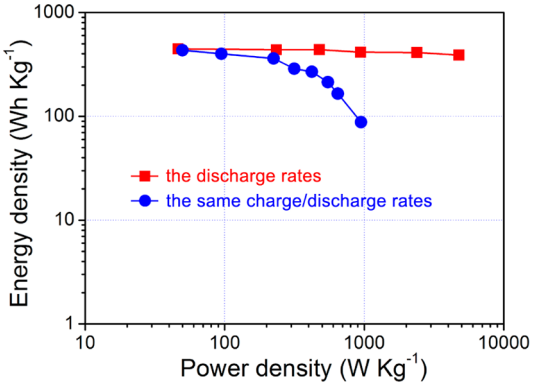

Figure 5. Ragone plots. Energy density as a function of power density for MnO/C nanopeapods in a Ragone plot under two discharge modes.

49.8 W kg^{-1}. When the power density is as high as 950 W kg^{-1}, the energy density of the hybrids can maintain 88.1 Wh kg^{-1}. It is noteworthy that the energy density can strikingly reach 389.3 Wh kg^{-1} at a super high power density of 4777 W kg^{-1} under a constant charge density of 100 mA g^{-1}. The power and energy densities are higher than other MnO-based materials reported by several groups on the basis of half-cell test.[10,13,30,31] The excellent electrochemical performance makes it a promising electrode for fabricating LIB devices with high power and energy densities.

The heterostructured MnO/C nanopeapods also possess excellent cyclic stability. Figure 6a shows the discharge capacity *versus* cycle number and the

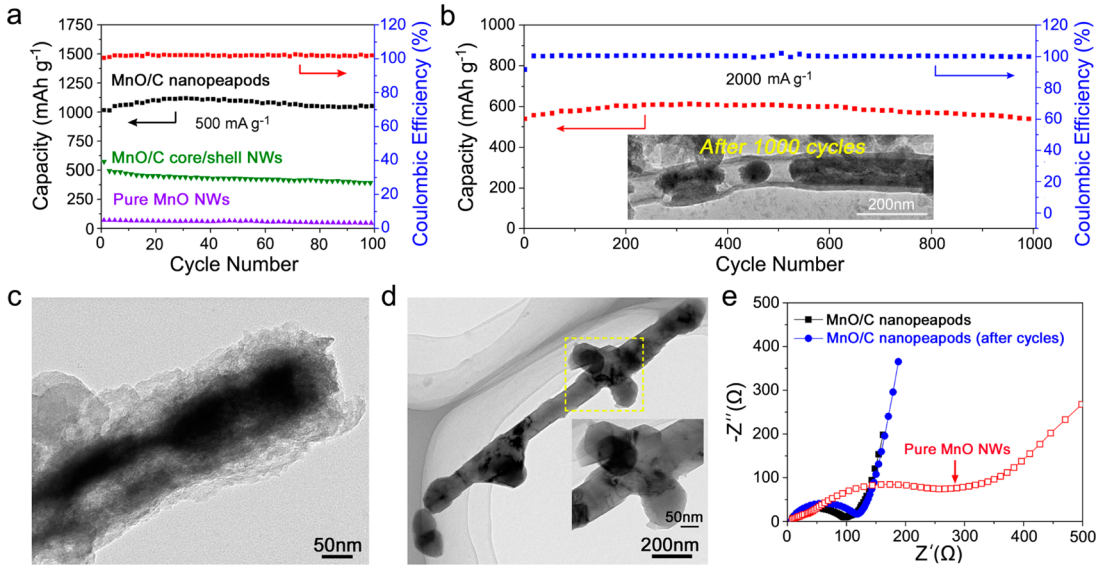

Figure 6. (a) Cycling performance of the MnO NWs, MnO/C core/shell NWs and MnO/C nanopeapods at 500 mA g^{-1} for 100 cycles, (b) cycling performance of the MnO/C nanopeapods at 2000 mA g^{-1} for 1000 cycles (the inset showing the TEM image of MnO/C nanopeapods after over 1000 cycles), (c,d) TEM images of MnO/C core/shell NWs (c) and MnO NWs (d) after 100 cycles, (e) electrochemical impedance spectra of the MnO/C nanopeapods before and after cycling and pure MnO.

corresponding Coulombic efficiency at a constant rate of 500 mA g^{-1}. The initial reversible capacity of the nanopeapods is up to 1018 mAh g^{-1}, which gradually reaches a maximum value of 1119 mAh g^{-1} after about 20 cycles, and then almost keeps the same for the next 80 cycles. Figure 6b shows the long-term cycles of the MnO/C peapods at a very high rate of 2000 mA g^{-1}. After 1000 cycles, the reversible capacity still retains a high value of 525 mAh g^{-1}. It is noted that the capacity of the MnO/C peapods at 2000 mA g^{-1} also shows an increasing trend at the beginning. This phenomenon is probably associated with either the formation of the SEI film or the high oxidation-state product, as demonstrated in recent reports on MnO-based materials for LIBs.[10,11,13,25] At the same time, a nearly 100% of Coulombic efficiency is achieved throughout the overall cycling operation. To the best of our knowledge, the best cycle performance of MnO anode materials in the literature so far delivered 650 mA h g^{-1} at 35.5 mA g^{-1} after 150 cycles while the power performance was not remarkable (210 mA h g^{-1} at 1600 mA g^{-1}).[11] Very recently, porous MnO/C core/shell NWs have been reported to possess a higher cycle stability, *i.e.*, 618.3 mAh g^{-1} after 200 cycles at 500 mA g^{-1} and higher rate performance, *i.e.*, 302.5 mAh g^{-1} at 3150 mA g^{-1}.[32] We further summarized detailed electrochemical performance of various reported MnO-based anodes for easy comparison (Table S2, Supporting Information). It is obvious that our MnO/carbon peapods exhibit overwhelming advantages considering capacity, rate performance and cycling life.

TEM image of the MnO/C nanopeapods after over 1000th charging (the inset of Figure 6b and Figure S10, Supporting Information) and discharging (Figure S11, Supporting Information) is provided, which turns out to be a direct proof of the structural stability and integrity of the material. No pulverization or size variation is observed, indicating that such smart heterostructure can indeed rise the function of relieving the strain and stress caused by volume variation and preventing the agglomeration or detachment of inner MnO NPs over cycling process. And also, we observe that the MnO/C nanopeapods expand mainly in axial direction after 1000 cycle. In view of the carbon shell protection, the expansion in radial direction is not remarkable. Therefore, the MnO/C nanopeapod morphology can be well-maintained during charge and discharge process. The structures of MnO/C core/shell NWs and MnO NWs after only 100 cycles were also investigated, as shown in Figure 6c (or Figure S12a, Supporting Information) and Figure 6d (or Figure S12b,c, Supporting Information), respectively. It is observed that some of MnO materials have been lost from NWs after only 100 cycles. These results indicate that the MnO/C nanopeapods with internal void space can offer enough room, which could effectively accommodate the volume variation during Li^+ insertion/extraction. Furthermore, the XPS spectra of the MnO/C core/shell NWs after 100 cycles have also been provided in Figure S13 (Supporting Information), which show almost the similar results as those of the MnO/C nanopeapods, indicating that the improvement of cycling stability is more related to the unique MnO/C nanopeapod structure.

The electrochemical impedance spectra (Figure 6e) of the MnO/C nanopeapods (■) and the pure MnO NWs (□) reveal that the MnO/C nanopeapods demonstrate a much lower resistance (~90.2 Ω) than the pure MnO NWs (~317.0 Ω). Such a reduction is owing to the existence of the conductive carbon shell. The electrochemical impedance spectrum of the MnO/C

nanopeapods after over 1000 cycles was also measured (●). The charge transfer resistance (~112.2 Ω) is just a little bit larger than that before cycling, further suggesting the high structural integrity.

DISCUSSION

The high initial Coulomb efficiency of ~88% on MnO/C nanopeapods can be mainly attributed to the obvious activation process at initial stage and the limited production of SEI by the introduction of carbon shell.[33,34] From the rate performance tests of the MnO/C nanopeapods (Figure 4b), it can be observed that the specific capacity slowly increases in the first 5 cycles at a current density of 100 mA g^{-1}. The result indicates that the MnO/C nanopeapods underwent an obvious activation process during the initial charge and discharge process, which is beneficial for improving the initial Coulombic efficiency. Furthermore, in view of the unique peapod-like structure, the Li ion may diffuse into the interior void space through the mesoporous pores of carbon shell during the repeated charge and discharge process, which would lead to the slow increase of specific capacity in the initial cycles.[33,34] In addition, the carbon shell can effectively limit the formation of SEI during initial charge and discharge process.

The unique nanoscale architecture of MnO/C nanopeapods is necessary and important for the exceptional electrochemical lithium storage capability. In the MnO/C nanopeapods, all the MnO NPs adhere onto the inner surface of CNTs, leading to large contact surface and good adherence. This helps to build good electrical connection with the conducting carbon, which has been verified by EIS results (Figure 6e). Furthermore, the MnO NPs confined in CNTs are well separated and do not aggregate even at a very high MnO content (~83.9%), guaranteeing a high weight capacity. These features lead to a higher capacity than MnO/C core/shell NWs and MnO NWs. In the case of stability, the pulverization of MnO NWs occurs during lithiation and battery cycling (Figure 6d). Despite thin carbon shell (~12 nm) in MnO/C core/shell NWs (Figure S6, Supporting Information) can in part reduce the pulverization of MnO and their etching from electrolyte (Figure 6c), the inevitable carbon cracking of MnO/C core/shell NWs during lithiation results in their limited stability. The MnO/C nanopeapods have empty internal void space, estimated to be ~20.6% by TEM, which is sufficient for MnO volumetric expansion without cracking the carbon layer, hence preserving the structural integrity and minimizing MnO dissolution. The direct evidence is from the TEM image of MnO/C nanopeapod after over 1000 cycles (the inset of Figure 6b and Figures S10 and S11, Supporting Information). We found that the nanopeapod morphology has been well-maintained after long-term stability test. Therefore, the internal void space of MnO/C nanopeapods can promise their good stability. Furthermore, unique structure of MnO/C nanopeapods can assist in the formation of a stable SEI. Electrochemical impedance spectra of the MnO/C nanopeapod electrode before and after *over 1000 cycles* (Figure 6e) show no conspicuous impedance increase, implying the limited growth of the SEI film, hence leading to the good cycling performance.[35,36]

CONCLUSION

In summary, the MnO NPs confined in CNTs with a peapod-like morphology have been successfully fabricated through a self-polymerization of dopamine on the surface of MnO-P NWs, and the subsequent carbonization of PDA as well as confined pyrolysis-*in situ* reduction process of the core material. As the MnO-P NWs showed the relatively poor crystallization, they could easily break into NPs during the high-temperature annealing treatment in inert gas, creating large void space of 20.6% between the MnO NPs inside CNTs. Such MnO/C nanopeapods could be used as a new class of anode materials for developing LIBs with high power density and extremely high stability. Compared with MnO NWs (149 mAh g^{-1}) and MnO/C core/shell NWs (547 mAh g^{-1}), the as-synthesized smart MnO/C nanopeapods exhibit a much higher specific capacity of 1119 mAh g^{-1} at 500 mA g^{-1} with excellent charge/discharge rate capability (rapidly charged to 91.6% in 10.6 min and 83.1% in 4.9 min at 500 mA g^{-1}). More remarkably, they have very high stability for LIBs. Their specific capacity can be well-maintained (almost no capacity fading) after cycling 1000 times at a high rate of 2000 mA g^{-1}. And there is no morphology change on the nanopeapod structure after the cycles. Such excellent electrochemical performance endows the MnO/C nanopeapods great potential as an anode material for LIBs. The strategy in this study not only represents a promising avenue for developing high performance MnO-based anode materials, but also can be easily extended to the fabrication of other anode and cathode materials for next-generation LIBs.

EXPERIMENTAL SECTION

Chemicals and Materials. All the reagents used in the experiment were of analytical grade (Sigma-Aldrich) and were used without further purification.

Synthesis of the MnO/C Nanopeapods. In a typical synthesis, 50 mg of polyvinylpyrrolidone (PVP) and 40 mL of 0.015 M $KMnO_4$ aqueous solution were mixed with magnetic stirring, and then the mixture was transferred into a 50 mL Teflon-lined stainless autoclave. The autoclave was sealed and put in an electronic oven at 160 °C for 9 h and then naturally cooled down to room temperature. The precipitates were collected by filtration, washed with deionized water and absolute ethanol, and finally redispersed in 50 mL of distilled water containing 40 mg of PEO-PPO-PEO (P123) and 60 mg of 2-amino-2-hydroxymethylpropane-1,3-dio

(Tris). After that, 20 mg of dopamine was added with continuous stirring in air for about 5 h. Similarly, the precipitates were collected by filtration, washed with deionized water and absolute ethanol and dried at 60 °C. Finally, the resulting products were annealed in argon at 900 °C for 2 h to prepare MnO/C nanopeapods (please note that the use of 900 °C can reduce MnO_x into MnO completely).

Synthesis of the MnO NWs. The MnO NWs were synthesized according to the report by Shen *et al.* with a minor modification.[19] In a typical procedure, 100 mg of PVP, 80 mg of $KMnO_4$ and 396 mg of $MnCl_2 \cdot 4H_2O$ were dissolved in 15 mL of distilled water, and then 0.5 mL of H_2O_2 (wt. 30%) was dropwise added. After magnetic stirring for 30 min, 10 mL of 0.12 M Li_2CO_3 aqueous solution was added. The mixture was further transferred to a 50 mL Teflon-lined stainless autoclave. The autoclave was kept at 180 °C for 24 h and then naturally cooled down to room temperature. The precipitates were collected by filtration, washed with deionized water and absolute ethanol and dried in a vacuum over at 60 °C. After annealing in argon at 600 °C for 5 h, the MnO NWs were obtained.

Synthesis of the MnO/C Core/Shell NWs. Similarly, the above MnO NWs (40 mg) were redispersed in 50 mL of distilled water containing 40 mg of PEO-PPO-PEO (P123) and 60 mg of 2-amino-2-hydroxymethylpropane-1,3-dio (Tris). After that, 20 mg of dopamine was added with continuous stirring in air for about 5 h. The precipitates were collected by filtration, washed several times with absolute ethanol and dried at 60 °C. Finally, the resulting product was annealed in argon at 900 °C for 2 h to prepare MnO/C core/shell NWs.

Characterization. The structure and morphology of as-prepared products were characterized with X-ray powder diffractometer (XRD; Rigaku D/Max 2550, Cu Kα radiation) at a scan rate of 1 °C min^{-1}, scanning electron microscopy (FESEM; Hitachi, S-4800, 15 kV), and transmission electron microscopy (TEM; JEOL, JEM-2100F) operated at 200 kV equipped with an X-ray energy dispersive spectrometer (EDS). The inductively coupled plasma (ICP) elemental analyses were performed from Optical Emission Spectrometer (Agilent 725ES). N_2 adsorption/desorption curve was determined by Brunauer–Emmett–Teller (BET) measurements using a Micromeritics ASAP 2010 surface area analyzer. Thermogravimetric analysis (NETZSCH STA409PC) was carried out with a heating rate of 10 °C min^{-1} under flowing air. Raman spectrum was recorded at ambient temperature with a NEXUS 670 FT-IR Raman spectrometer.

Electrochemical Measurements. Electrochemical measurements were performed using coin-type 2016 cells. The working electrode was prepared as follows. First the as-synthesized active materials, carbon black, and poly(vinyl difluoride) (PVDF) were mixed in NMP with a weight ratio of 80:10:10, and then the slurry was pasted onto pure Cu foil. The electrolyte consists of a solution of 1 M $LiPF_6$ in ethylene carbonate (EC)/dimethyl carbonate (DMC) (volume ratio of 1:1). Pure lithium foil was used as counter electrode, and the separator was a polypropylene membrane from Celgard. The coating thickness on Cu foil is about 80 μm. The mass loading of the active materials is about 0.6 mg. The cells were assembled in an argon-filled glovebox. The charge and discharge performances were carried out on a LAND-CT2001C test system within a range of 0.02–3 V at different current densities. Cyclic voltammogram experiment was performed on an Autolab PGSTAT302N electrochemical workstation at a scan rate of 0.1 mV s^{-1}.

Conflict of Interest: The authors declare no competing financial interest.

Acknowledgment. This work was supported by the National Natural Science Foundation of China (21136006, 21206043, 21236003), the Research Project of Chinese Ministry of Education (113026A), the Shanghai Pujiang Program (12PJ1401900), the Shanghai Rising-Star Program (13QA1401100), Program for Professor of Special Appointment (Eastern Scholar) at Shanghai Institutions of Higher Learning, Fundamental Research Funds for the Central Universities, and J. Robert Oppenheimer distinguished fellowship.

Supporting Information Available: Figures S1–S13 and Tables S1 and S2. This material is available free of charge *via* the Internet at http://pubs.acs.org.

REFERENCES AND NOTES

1. Kang, B.; Ceder, G. Battery Materials for Ultrafast Charging and Discharging. *Nature* **2009**, *458*, 190–193.
2. Dunn, B.; Kamath, H.; Tarascon, J. M. Electrical Energy Storage for the Grid: a Battery of Choices. *Science* **2011**, *334*, 928–935.
3. Park, C. M.; Kim, J. H.; Kim, H.; Sohn, H. J. Li-Alloy Based Anode Materials for Li Secondary Batteries. *Chem. Soc. Rev.* **2010**, *39*, 3115–3141.
4. Jiang, H.; Ma, J.; Li, C. Z. Mesoporous Carbon Incorporated Metal Oxide Nanomaterials as Supercapacitor Electrodes. *Adv. Mater.* **2012**, *24*, 4197–4202.
5. Hu, L. H.; Wu, F. Y.; Lin, C. T.; Khlobystov, A. N.; Li, L. J. Inhibition of PDE4B Suppresses Inflammation by Increasing Expression of the Deubiquitinase CYLD. *Nat. Commun.* **2013**, *4*, 1684–1696.
6. Jang, B.; Park, M.; Chae, O. B.; Park, S.; Kim, Y.; Oh, S. M.; Piao, Y.; Hyeon, T. Direct Synthesis of Self-Assembled Ferrite/Carbon Hybrid Nanosheets for High Performance Lithium-Ion Battery Anodes. *J. Am. Chem. Soc.* **2012**, *134*, 15010–15015.
7. Chan, C. K.; Peng, H. L.; Liu, G.; McIlwrath, K.; Zhang, X. F.; Huggins, R. A.; Cui, Y. High-Performance Lithium Battery Anodes Using Silicon Nanowires. *Nat. Nanotechnol.* **2008**, *3*, 31–35.
8. Jiao, F.; Bruce, P. G. Mesoporous Crystalline β-MnO_2—A Reversible Positive Electrode for Rechargeable Lithium Batteries. *Adv. Mater.* **2007**, *19*, 657–660.
9. Pan, A. Q.; Wu, H. B.; Yu, L.; Lou, X. W. Template-Free Synthesis of VO_2 Hollow Microspheres with Various Interiors and Their Conversion into V_2O_5 for Lithium-Ion Batteries. *Angew. Chem., Int. Ed.* **2013**, *52*, 2226–2230.
10. Xia, Y.; Xiao, Z.; Dou, X.; Huang, H.; Lu, X. H.; Yan, R. J.; Gan, Y. P.; Zhu, W. H.; Tu, J. P.; Zhang, W. K.; *et al.* Green and Facile Fabrication of Hollow Porous MnO/C Microspheres from Microalgaes for Lithium-Ion Batteries. *ACS Nano* **2013**, *7*, 7083–7092.
11. Zhong, K. F.; Xia, X.; Zhang, B.; Li, H.; Wang, Z. X.; Chen, L. Q. MnO Powder as Anode Active Materials for Lithium Ion Batteries. *J. Power Sources* **2010**, *195*, 3300–3308.
12. Sun, B.; Chen, Z. X.; Kim, H. S.; Ahn, H. G.; Wang, X. MnO/C Core–Shell Nanorods as High Capacity Anode Materials for Lithium-Ion Batteries. *J. Power Sources* **2011**, *196*, 3346–3349.
13. Chen, W. M.; Qie, L.; Shen, Y.; Sun, Y. M.; Yuan, L. X.; Hu, X. L.; Zhang, W. X.; Huang, Y. H. Superior Lithium Storage Performance in Nanoscaled MnO Promoted by N-Doped Carbon Webs. *Nano Energy* **2013**, *2*, 412–418.
14. Li, X. W.; Li, D.; Qiao, L.; Wang, X. H.; Sun, X. L.; Wang, P.; He, D. Y. Interconnected Porous MnO Nanoflakes for High-Performance Lithium Ion Battery Anodes. *J. Mater. Chem.* **2012**, *22*, 9189–9194.
15. Ding, Y. L.; Wu, C. Y.; Yu, H. M.; Xie, J. G.; Cao, S.; Zhu, T. J.; Zhao, X. B.; Zeng, Y. W. Coaxial MnO/C Nanotubes as Anodes for Lithium-Ion Batteries. *Electrochim. Acta* **2011**, *56*, 5844–5848.
16. Sun, Y. M.; Hu, X. L.; Luo, W.; Xia, F. F.; Huang, Y. H. Reconstruction of Conformal Nanoscale MnO on Graphene as a High-Capacity and Long-Life Anode Material for Lithium Ion Batteries. *Adv. Funct. Mater.* **2013**, *23*, 2436–2444.
17. Hsieh, C. T.; Lin, C. Y.; Lin, J. Y. High Reversibility of Li Intercalation and De-Intercalation in MnO-Attached Graphene Anodes for Li-Ion Batteries. *Electrochim. Acta* **2011**, *56*, 8861–8867.
18. Liu, Y. M.; Zhao, X. Y.; Li, F.; Xia, D. G. Facile Synthesis of MnO/C Anode Materials for Lithium-Ion Batteries. *Electrochim. Acta* **2011**, *56*, 6448–6452.
19. Shen, X. P.; Ji, Z. Y.; Miao, H. J.; Yang, J. K.; Chen, M. Hydrothermal Synthesis of $MnCO_3$ Nanorods and Their Thermal Transformation into Mn_2O_3 and Mn_3O_4 Nanorods with Single Crystalline Structure. *J. Alloys Compd.* **2011**, *509*, 5672–5676.
20. Zhang, K. J.; Han, P. X.; Gu, L.; Zhang, L. X.; Liu, Z. H.; Kong, Q. S.; Zhang, C. J.; Dong, S. M.; Zhang, Z. Y.; Yao, J. H.; *et al.* Synthesis of Nitrogen-Doped MnO/Graphene Nanosheets Hybrid Material for Lithium Ion Batteries. *ACS Appl. Mater. Interfaces* **2012**, *4*, 658–664.

21. Kang, E.; Jung, Y. S. G.; Kim, H.; Chun, J. Y.; Wiesner, U.; Dillon, A. C.; Kim, J. K.; Lee, J. Highly Improved Rate Capability for a Lithium-Ion Battery Nano-$Li_4Ti_5O_{12}$ Negative Electrode *via* Carbon-Coated Mesoporous Uniform Pores with a Simple Self-Assembly Method. *Adv. Funct. Mater.* **2011**, *21*, 4349–4357.
22. He, C. N.; Wu, S.; Zhao, N. Q.; Shi, C. S.; Liu, E. Z.; Li, J. J. Carbon-Encapsulated Fe_3O_4 Nanoparticles as a High-Rate Lithium Ion Battery Anode Material. *ACS Nano* **2013**, *7*, 4459–4469.
23. Wu, M.; Chiang, S. P. C. J. Electrochemically Deposited Nanowires of Manganese Oxide as an Anode Material for Lithium-Ion Batteries. *Electrochem. Commun.* **2006**, *8*, 383–388.
24. Yu, X. Q.; He, Y.; Sun, J. P.; Tang, K.; Li, H.; Chen, L. Q.; Huang, X. J. Nanocrystalline MnO Thin Film Anode for Lithium Ion Batteries with Low Overpotential. *Electrochem. Commun.* **2009**, *11*, 791–794.
25. Mai, Y. J.; Zhang, D.; Qiao, Y. Q.; Gu, C. D.; Wang, X. L.; Tu, J. P. MnO/Reduced Graphene Oxide Sheet Hybrid as an Anode for Li-Ion Batteries with Enhanced Lithium Storage Performance. *J. Power Sources.* **2012**, *216*, 201–207.
26. Delmer, O.; Balaya, P.; Kienle, L.; Maier, J. Enhanced Potential of Amorphous Electrode Materials: Case Study of RuO_2. *Adv. Mater.* **2008**, *20*, 501–505.
27. Li, X. N.; Zhu, Y. C.; Zhang, X.; Liang, J. W.; Qian, Y. T. MnO@1-D Carbon Composites from the Precursor $C_4H_4MnO_6$ and Their High-performance in Lithium Batteries. *RSC Adv.* **2013**, *3*, 10001–10006.
28. Guo, J. C.; Liu, Q.; Wang, C. S.; Zachariah, M. R. Interdispersed Amorphous MnO_x—Carbon Nanocomposites with Superior Electrochemical Performance as Lithium-Storage Material. *Adv. Funct. Mater.* **2012**, *22*, 803–811.
29. Wang, H. L.; Cui, L. F.; Yang, Y.; Casalongue, H. S.; Robinson, J. T.; Liang, Y. Y.; Cui, Y.; Dai, H. J. Mn_3O_4—Graphene Hybrid as a High-Capacity Anode Material for Lithium Ion Batteries. *J. Am. Chem. Soc.* **2010**, *132*, 13978–13980.
30. Wang, S. B.; Ren, Y. B.; Liu, G. R.; Xing, Y. L.; Zhang, S. C. Peanut-like MnO@C Core-Shell Composites as Anode Electrodes for High-performance Lithium Ion Batteries. *Nanoscale* **2014**, *6*, 3508–3512.
31. Liu, B.; Hu, X. L.; Xu, H. H.; Luo, W.; Sun, Y. M.; Huang, Y. H. Encapsulation of MnO Nanocrystals in Electrospun Carbon Nanofibers as High-Performance Anode Materials for Lithium-Ion Batteries. *Sci. Rep.* **2014**, *4*, 4229–4234.
32. Xu, G. L.; Xu, Y. F.; Sun, H.; Fu, F.; Zheng, X. M.; Huang, L.; Li, J.; Yang, T. S. H.; Sun, S. G. Facile Synthesis of Porous MnO/C Nanotubes as a High Capacity Anode Material for Lithium Ion Batteries. *Chem. Commun.* **2012**, *48*, 8502–8504.
33. Shimoda, H.; Gao, B.; Tang, X. P.; Kleinhammes, A.; Fleming, L.; Wu, Y.; Zhou, O. Lithium Intercalation into Opened Single-Wall Carbon Nanotubes: Storage Capacity and Electronic Properties. *Phys. Rev. Lett.* **2002**, *88*, 015502.
34. Sun, J.; Liu, H. M.; Chen, X.; Evans, D. G.; Yang, W. S.; Duan, X. Carbon Nanorings and Their Enhanced Lithium Storage Properties. *Adv. Mater.* **2013**, *25*, 1125–1130.
35. Liu, S. Y.; Xie, J.; Zheng, Y. X.; Cao, G. S.; Zhu, T. J.; Zhao, X. B. Nanocrystal Manganese Oxide (Mn_3O_4, MnO) Anchored on Graphite Nanosheet with Improved Electrochemical Li-Storage Properties. *Electrochim. Acta* **2012**, *66*, 271–278.
36. Wu, H.; Yu, G. H.; Pan, L. J.; Liu, N. M.; McDowell, T.; Bao, Z. N.; Cui, Y. Stable Li-Ion Battery Anodes by *In-Situ* Polymerization of Conducting Hydrogel to Conformally Coat Silicon Nanoparticles. *Nat. Commun.* **2013**, *4*, 1943–1948.